Physica Medica 60 (2019) 132–138

Contents lists available at ScienceDirect

Physica Medica

journal homepage: www.elsevier.com/locate/ejmp

Original paper

Effect of low magnetic field on single-diode dosimetry for clinical use

Chang Heon Choi[a,b,c], Jong Min Park[a,b,c,d], Hyun Joon An[a,b,c], Jung-in Kim[a,b,c,*]

[a] Department of Radiation Oncology, Seoul National University Hospital, Seoul, Republic of Korea
[b] Institute of Radiation Medicine, Seoul National University Medical Research Center, Seoul, Republic of Korea
[c] Biomedical Research Institute, Seoul National University Hospital, Seoul, Republic of Korea
[d] Center for Convergence Research on Robotics, Advanced Institutes of Convergence Technology, Suwon, Republic of Korea

ARTICLE INFO

Keywords:
MR-IGRT
QED detector
Diode detector
In vivo dosimetry

ABSTRACT

Purpose: To evaluate the effect of a low magnetic field (B-field, 0.35 T) on QED™ for clinical use.
Methods: Black and Blue QED were irradiated using tri-Co-60 magnetic resonance image-guided radiation therapy systems with and without the B-field. For both detectors, angular dependence of the beam orientation was evaluated by rotating the gantry and detector in *parallel* and *perpendicular* directions to the B-field. Angular dependence between the directions of both QED and B-field was also measured. Response on the depth and output factor of both detectors was investigated for *parallel* and *perpendicular setups*, respectively.
Results: When Black QED was placed on a surface, detector response decreased by 1.8% and 4.5% for *parallel* and *perpendicular setups*, respectively, owing to the B-field. The angular dependence of the beam orientation was not affected by B-field for both detectors. There was a significant angular dependence between Black QED and B-field direction and for the Black QED when the gantry was rotated. Owing to the B-field, the detector response at 90° decreased by 2.4%, response of Black QED on the depth was changed only on the surface, and output factor of Black QED was changed only on the surface. The response of Blue QED was not affected by the B-field for all examined situations.
Conclusions: Using Black QED on a surface in the same position as that in the calibration requires some correction to the B-field. Blue QED does not require correction as it is not affected by the B-field.

1. Introduction

Modern radiation therapy aims to concentrate the dose to the tumor while sparing the surrounding normal tissues [1]. For instance, intensity-modulated radiation therapy (IMRT) and volumetric arc therapy achieve this purpose by generating high conformal dose distributions [2]. However, tumors can be located very close to normal organs, such as the rectum and the bladder in prostate cancer, the brain stem in brain cancer, the parotid grand and optic chiasm in nasopharynx cancer, and the spinal cord in spine cancer. In these cases, the normal organ can be included in the planning target volume, which defines a margin to account for positioning uncertainty and internal organ motion [3,4], thus generating a conflict between tumor dose and normal tissue tolerance [5,6]. Therapeutic dose is limited to reduce the probability of complication, and local control can fail during radiation therapy [7]. To overcome these problems, researchers have introduced image-guided radiation therapy (IGRT), which reduces the planning target volume margin [8,9].

The integration of magnetic resonance imaging (MRI) into radiation treatment systems provides a high onboard tumor visibility with superior soft-tissue contrast compared to that of conventional computed tomography [10,11]. Magnetic resonance image-guided radiation therapy (MR-IGRT) applications have become clinically available. For instance, the ViewRay™ system (ViewRay Technologies, Inc., Cleveland, OH, USA) delivers a field strength of 0.35 T for MR-IGRT [12,13], enables static IMRT with multileaf collimators (MLCs, 1.05 cm in width at 105 cm from the source) [14], and has provided clinically proven outcomes [15–19]. The presence of magnetic field with respect to the radiation beam in systems integrated with MRI affects these contaminant electrons, resulting in changes in dose deposition due to the Lorentz force [20,21]. The dosimetric characteristics of each detector under a magnetic field should be investigated before clinical use. Previous studies have reported on the effect of strong magnetic fields on dosimetry devices including ionization chambers, film and plastic scintillators, optically stimulated luminescent dosimeters, diode detectors, EBT3 films, and PRESAGE® gel (Heuris, Inc., Skillman, NJ, USA) [20–24].

In vivo dosimetry can be used to improve the treatment efficacy by

* Corresponding author at: Department of Radiation Oncology, Seoul National University Hospital, Seoul 03080, Republic of Korea.
E-mail address: madangin@gmail.com (J.-i. Kim).

https://doi.org/10.1016/j.ejmp.2019.04.001
Received 13 September 2018; Received in revised form 18 March 2019; Accepted 1 April 2019
Available online 04 April 2019

verifying the external beam in the radiation therapy [25]. Various dosimeters (e.g., TLD, OSLD, film, metal oxide-silicon semiconductor field effect transistors, and semiconductor diodes) have been available for in vivo dosimetry [25]. These detectors can be positioned on the surface or inserted into the body cavities of patients [26]. Diode detectors are also being widely used for in vivo dosimetry owing to their short processing time and high sensitivity. In addition, diode detectors have outstanding features, high reproducibility, mechanical stability, absence of external bias, small size, and energy independence from mass-collision stopping-power ratios, making them suitable for clinical use [25,27]. O'Brien et al. reported on the response of commercially available diode detectors (e.g., PTW 60,016 Diode P and 60,018 Diode SRS, PTW, Freiburg, Germany) and of the IBA PFD diode detector (IBA Dosimetry, Schwarzenbruck, Germany) using an MRI-LINAC system [28]. However, these detectors cannot be applied for in vivo dosimetry owing to their cylindrical shape. In contrast, the QED™ detectors (Sun Nuclear Corporation, Melbourne, FL, USA) are available for clinical use, especially for in vivo dosimetry [25,29].

Under the condition without the effects of a magnetic field, the dosimetric characteristics of QED detectors were investigated. QED detectors have good reproducibility, but need periodic checking of their calibration factor [25,29]. The angular dependence of QED detectors has been reported to be as high as 14% for large gantry angles [25,29]. In addition, QED detectors have source-to-surface distance (SSD), field size, and wedge dependencies and all of their correction factors should be verified [30].

However, the dosimetry characteristics of these detectors have not yet been investigated in the presence of magnetic fields for in vivo dosimetry. During an actual radiation treatment of an individual patient, the surface or the part close to the patient's anatomy needs to be verified for quality assurance.

With the presence of magnetic field, these contaminant electrons generated in the patient's body surface can spread out along the direction of the magnetic field [31]. QED detectors, which are usually used to measure the dose on the body, can be affected by the dose deposited from these contaminant electrons. Because QED detectors have been used with a bolus to provide a build-up region and to insert them into the body cavities of patients, the effect of the electron on the depth should be examined.

In this study, we investigated the response of QED detectors (positive output diode detectors) for in vivo dosimetry use under 0.35 T of magnetic field. Specifically, we evaluated the angular, magnetic field direction, and field size dependencies, as well as the dose at the surface and at depths of 1 cm and 5 cm.

2. Materials and methods

2.1. QED detectors and calibration

The QED detectors are made from proprietary radiation-hardened silicon diodes, whose die is surface mounted on an FR4 glass reinforced with epoxy resin and is located at the center of the circular area [32]. In addition, the die plane is parallel to the circular area, and the build-up materials are mounted above the die conforming to height h and to bottom surface diameter D, as shown in Fig. 1 [32]. For this study, black and blue QED detectors were selected by considering the Co-60 radiation source of the ViewRay system, which emits energies of 1.33 and 1.17 MeV. The characteristics of these detectors are listed in Table 1. The detectors were connected to an rf-IVD 2™ system (Sun Nuclear Corporation), which was located where it could not be affected by magnetic fields for dose reading and analysis. The detectors were calibrated using the ViewRay system to deliver a radiation dose of 1.0 Gy at the maximum build-up depth under normal conditions. The normal condition was defined as a gantry head of 0°, field size of $10.5 \times 10.5\ cm^2$, and SSD without a magnetic field of 105 cm. The detectors were attached on top of a phantom surface.

2.2. Tri-Co-60 system with an MR system

Three Co-60 sources with a 120° offset in a ring-type bore were installed in the ViewRay system. For the Co-60 irradiation, gantry head 1 or 3 was used depending on the allowed gantry angle. Gantry heads 1 and 3 were used from 0° to 90° and from 270° to 0°, respectively. At 0°, the output for both heads was the same. During irradiation, the normal activities for gantry heads 1 and 3 were 9965.79 and 9960.85 Ci, respectively, and the beam-on time was calculated to deliver 1 Gy of radiation dose to the detector at the isocenter. Measurements were performed both with and without the 0.35-T magnetic field. The electromagnet powered off for the condition without a magnetic field.

2.3. Angular dependence by gantry rotation (setups 1 and 2)

The measurement setup for the angular dependence is illustrated in Fig. 2. The angular dependence of the QED detectors was measured by rotating the gantry head over the diode. The diode was placed on top of a solid water phantom (Virtual Water™ Phantom; Radiation Products Design, Inc., Albertville, MN, USA) with 5-cm thickness to evaluate the angular dependence by rotating the gantry. To examine the orientation dependence of the magnetic field, we placed the QED detectors in parallel (Fig. 2(a), setup 1) and perpendicular (Fig. 2(b), setup 2) directions to the magnetic field. All measurement values were normalized according to the readings obtained under the normal condition for angular dependence by gantry rotation.

2.4. Angular dependence by detector rotation (setups 3 and 4)

In addition, the angular dependence of the QED detectors was also measured by rotating the diode with a fixed gantry head at 0°. To evaluate the angular dependence by rotating the diode, we fabricated a special holder using polymethyl methacrylate (PMMA) for each detector. The detector diode was positioned at the center of the rotation axis, and a distance of 105 cm between the diode center and the radiation source was maintained during the rotation. The holder was machined by using an acrylic laser cutting device according to the block diagram provided by the manufacturer. The QED detectors could be fitted tightly into the hole to eliminate any air gap between the holder and the detector as much as possible. They were also aligned in parallel (Fig. 2(c), setup 3) and perpendicular (Fig. 2(d), setup 4) directions to the magnetic field. The measurement of the angular dependency was normalized according to the readings obtained at a 0° angle of the holder of the diode detector.

2.5. Angular dependence between the QED detector orientation and the magnetic field direction (setup 5)

To measure the angular dependence between the QED detector direction and the magnetic field, we irradiated the detectors under seven different angles between 0° and 180° at increments of 30°, where 0° indicates that the QED detector is parallel to the magnetic field (Fig. 2(e)).

2.6. Responses on the depth

The response of the QED detectors upon varying the depth was measured to evaluate the variation of the detector characteristics based on the magnetic fields on the depth. The solid water phantom was stacked on top of the QED detectors to maintain the SSD. The measurements were performed at depths of 0 cm, 1 cm, and 5 cm. The response of the QED detectors was also examined in perpendicular (*perpendicular setup*) and parallel directions (*parallel setup*) to the magnetic field.

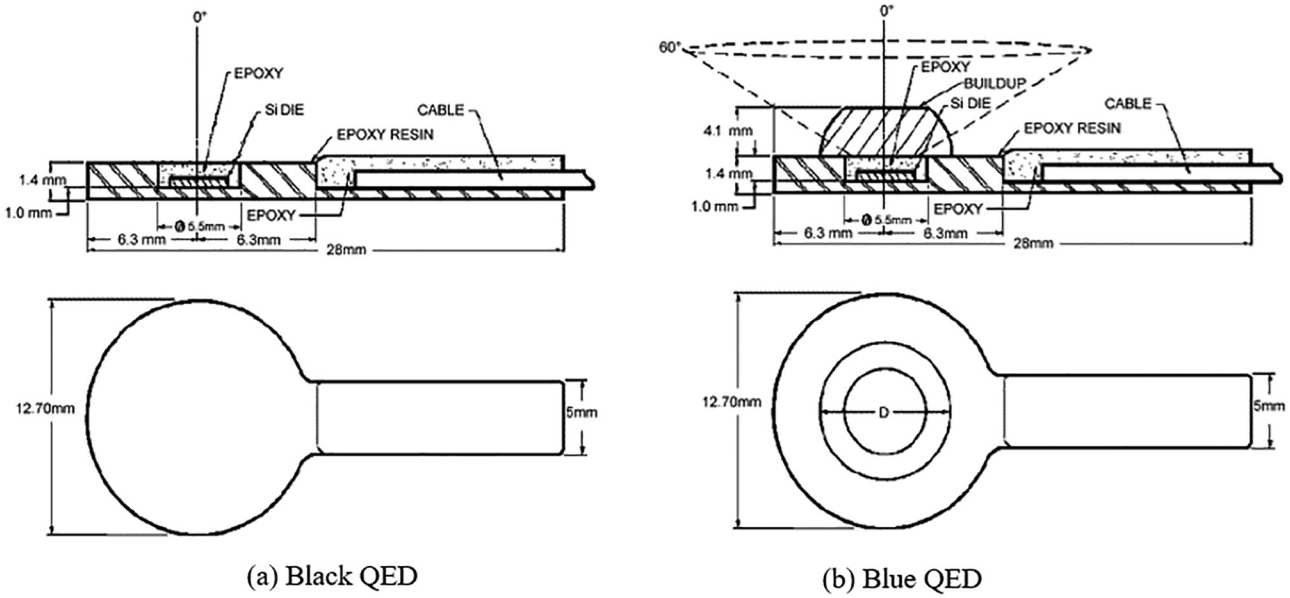

Fig. 1. Schematic top and cross-sectional views of the QED detector used for measuring the effect of magnetic fields (a). Buildup height *h* of the (b) black QED and (c) blue QED detectors is 0.0 mm and 3.4 mm, respectively [32].

Table 1
Characteristics of the QED detector diodes [28].

Color	Black	Blue
Voltage range	Skin	1–4 MV
Buildup material	None	Aluminum
Buildup (g/cm^2)	0.1	1.1
Energy for directional response	Co-60	Co-60
Diameter (*D*)	N/A	7.9 mm
Height (*h*)	N/A	3.4 mm
Area (mm^2)	0.64	
Active dimension (mm)	0.8 × 0.8	
Dose rate dependence	± 1%, 75–250 cm of source-to-surface distance	
Detector sensitivity (nC/Gy)	32	
Detector stability	0.5% per kilogray at 6 MV	

2.7. Output factors for the magnetic field direction and the magnetic field presence

The output factor was measured to estimate the response of the detectors upon varying the field size. The effect was measured with field sizes of 4.2 × 4.2 cm^2, 10.5 × 10.5 cm^2, 21.0 × 21.0 cm^2, and 27.3 × 27.3 cm^2 at the surface and at depths of 1 cm and 5 cm. These field sizes can be shaped by the MLC in the ViewRay system. The smallest field size that could be collimated using the MLC system was 2.1 × 2.1 cm^2. Because the ViewRay system has no flattening fitter, the flatness of the smallest field size was not appropriate to the size of the QED detectors. Therefore, we chose the field size of 4.2 × 4.2 cm^2 for the smallest field size.

The effect on the directions to the magnetic field of the output factor was also evaluated for the *perpendicular* and *parallel setups*.

3. Results

3.1. Absolute dose difference and measurement uncertainty

When a magnetic field was applied to setup 1, the absolute response of the black QED detector decreased by 1.8% for 0° of gantry angle, whereas the response of the blue QED detector did not change. The measurement uncertainty using the QED detectors was evaluated at 0.5% from three separate measurements.

3.2. Angular dependence by gantry rotation (setups 1 and 2)

Fig. 3 depicts the angular dependence of the two QED detectors by gantry rotation between the QED detector and the magnetic field direction with and without a magnetic field. For the black QED detector under setup 1 (Fig. 2(a)), the average difference was 2.0% for gantry angles 280° to 80°, and decreased by 1% for gantry angles 270° and 90° in the presence of magnetic fields. Regarding setup 2 shown in Fig. 2(b), the response of the black QED detector under a magnetic field was 4.5% lower, on average between all gantry angles, than that without a magnetic field. For the black QED detectors under setups 1 and 2 (i.e., different orientation), no difference was found for gantry angles 300° to 60° without a magnetic field, whereas differences of 25% and 21% were found for gantry angles 270° and 90°. However, with a magnetic field, the average difference was 2.6% for 290° to 70° of gantry angle and it increased by up to 33% and 24% for gantry angles 270° and 90°, respectively. For both setup 1 and setup 2, no difference in the response of the blue QED detector was observed in the presence of a magnetic field. However, the response of the blue QED detector, in setup 2 with and without B-field, decreased from 1.01 to 0.98 for gantry angles 280° to 80°. For gantry angles 270° and 90°, the detector response was decreased by 34.1% from the response at gantry angle of 0°.

3.3. Angular dependence by detector rotation (setups 3 and 4)

The angular dependence by detector rotation with a fixed gantry (setups 3 and 4) is shown in Fig. 4. The response decreased by about 15% and 5% from 0° to 90° for the black and the blue QED detector, respectively. The response of the black QED detector decreased sharply between 90° and 120°. For the blue QED detector, the response gradually decreased as the angle increased. The response of the blue QED detector decreased to 0.77 at 180°. However, the angular dependence was not affected by the magnetic field for both detectors.

3.4. Angular dependence between the detector orientation and the magnetic field direction (setup 5)

The angular dependence between the detector orientation and the magnetic field direction (setup 5) is listed in Table 2. The black QED detector showed a dependence on the magnetic field as its response

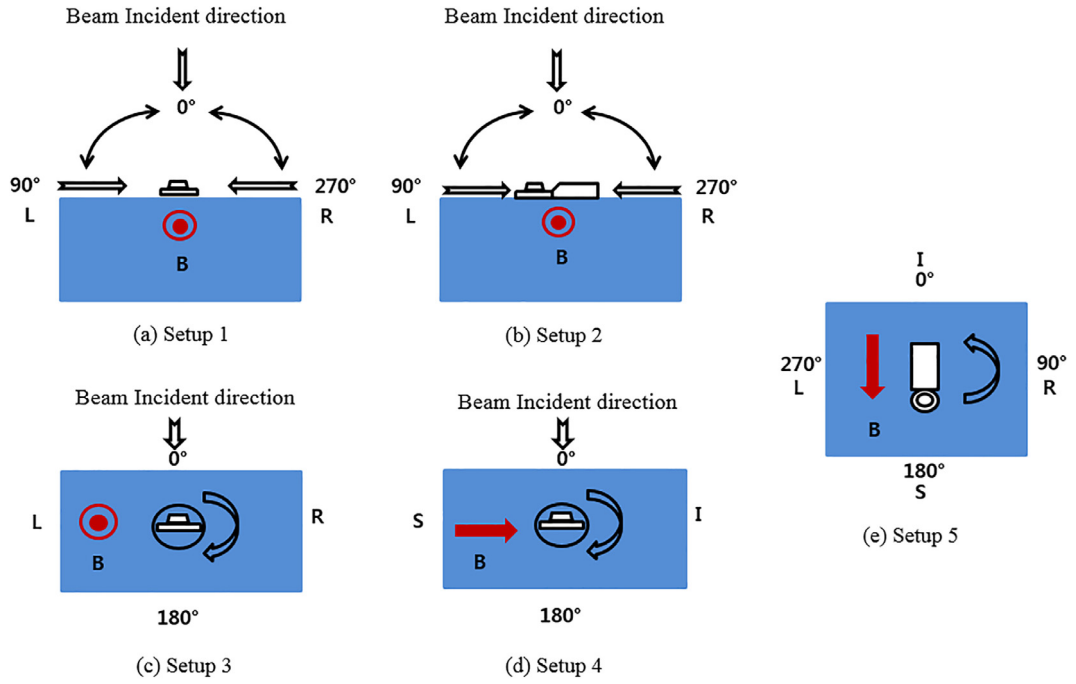

Fig. 2. Measurement setup for the detector and the incident beam with respect to the direction of the magnetic field. (a–e) show setups 1 to 5, respectively. The magnetic field is applied in the longitudinal direction (i.e., inferior (I) to superior (S)). The QED detector is fixed on the top of a solid water phantom during gantry rotation. The detector is placed (a) perpendicular and (b) parallel to the direction of the magnetic field. The QED detector is inserted into the PMMA holder for rotating. The detector is rotated (c) perpendicularly and (d) parallel to the direction of the magnetic field at a fixed gantry angle of 0°. (e) The detector is rotated counterclockwise on the surface of the solid water phantom at a fixed gantry angle in the top view (0°). (L: left; R: right; S: superior; I: inferior; B: magnetic field; ⊙: magnetic field pointing out of the page; red arrow: magnetic field direction.) (For interpretation of the references to color in this figure legend, the reader is referred to the web version of this article.)

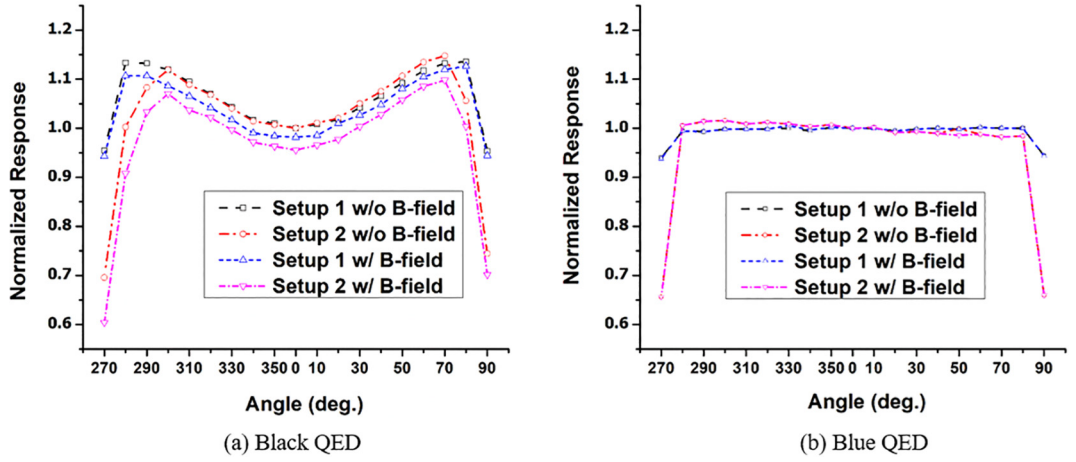

Fig. 3. Relative angular dependence by rotating the gantry. Dependency for the (a) black QED and (b) blue QED detectors. The lines with black squares and blue triangles indicate the absence and presence of a magnetic field under setup 1, respectively. The lines with red circles and magenta triangles indicate the absence and presence of a magnetic field under setup 2, respectively. (W/O B-field: without a magnetic field; W/ B-field: with a magnetic field.) (For interpretation of the references to color in this figure legend, the reader is referred to the web version of this article.)

decreased to 0.973 from 0° to 90°. The response was 1.000 at 180°. In contrast, no such variation was observed for the blue QED detector.

3.5. Responses on the depth

The responses of each QED detector on the depth are listed in Table 3 for the three evaluated depths. All measured data were normalized at 1-cm depth for each setup. The response of the black QED detector at the surface changed by 4.5% when the detector was placed under the *perpendicular setup* with a magnetic field. At 1-cm and 5-cm depths, the responses of the black QED detector were identical under the *perpendicular* and *parallel setups*. No other variation in the responses on the depth regarding the direction and presence of magnetic fields at the three depths occurred for the blue QED detector.

3.6. Output factors of the magnetic field direction and the magnetic field presence

Table 4 lists the output factors of both detectors according to field size depth, direction of magnetic field, and magnetic field presence. All measured data were normalized at a response field size of $10.5 \times 10.5\,cm^2$ for each setup. Only the output factors of the black

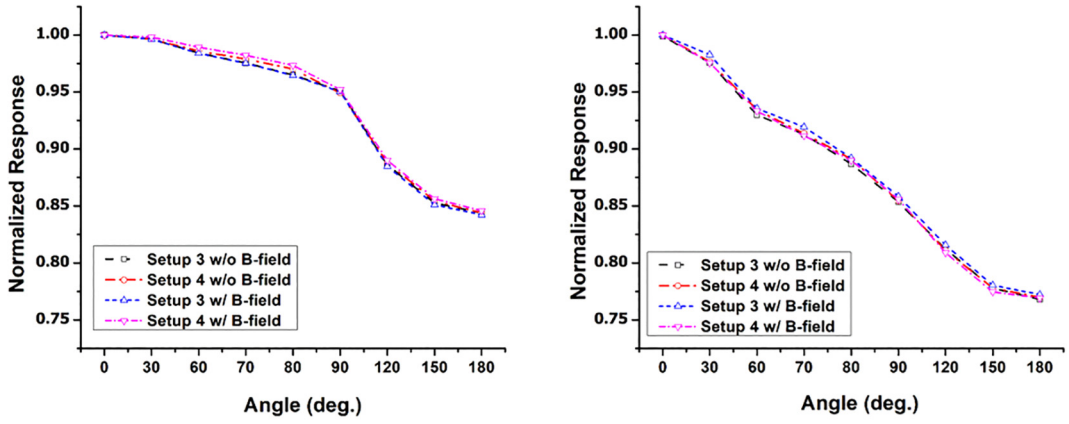

Fig. 4. Relative angular dependence by rotating the detector diode. Dependency for the (a) black QED and (b) blue QED detectors. The lines with black squares and blue triangles indicate the absence and presence of a magnetic field under setup 3, respectively. The lines with red circles and magenta triangles indicate the absence and presence of a magnetic field under setup 4, respectively. (W/O B-field: without a magnetic field; W/ B-field: with a magnetic field.) (For interpretation of the references to color in this figure legend, the reader is referred to the web version of this article.)

Table 2
Angular dependence between the QED detector and the magnetic field (B-field) direction ((e) setup 5 in Fig. 2).

Angle (°)	Black QED detector		Blue QED detector	
	Without a B-field	With a B-field	Without a B-field	With a B-field
0	1.000	1.000	1.000	1.000
30	1.001	0.981	1.000	1.000
60	1.001	0.976	1.000	1.000
90	1.000	0.973	1.000	1.000
120	1.000	0.995	1.000	1.000
150	1.000	0.985	1.000	1.000
180	0.999	1.002	1.000	1.000

Table 3
Response of the QED detector diodes on the surface and at depths of 1 cm and 5 cm for the magnetic field direction, with and without a magnetic field.

Depth	Parallel without a B-field	Perpendicular without a B-field	Parallel with a B-field	Perpendicular with a B-field
	Black QED			
Surface	0.753	0.753	0.739	0.719
1 cm	1.000	1.000	1.000	1.000
5 cm	0.885	0.885	0.884	0.885
	Blue QED			
Surface	1.009	1.009	1.008	1.008
1 cm	1.000	1.000	1.000	1.000
5 cm	0.902	0.902	0.902	0.902

QED detector varied on the surface with a magnetic field. When the black QED detector was under the *perpendicular setup*, its absolute response decreased by 0.5%, 2.7%, 3.8%, and 4.3% for four field sizes, respectively, compared to that under the *parallel setup*. At 1 cm and 5 cm depths, the response did not change with and without a magnetic field under the perpendicular setup.

Table 4
Output factor of the QED detector diodes on the surface and at depths of 1 cm and 5 cm for the magnetic field size and direction, with and without a magnetic field.

Field size (cm^2)	Parallel without a B-field	Perpendicular without a B-field	Parallel with a B-field	Perpendicular with a B-field
	Black QED			
	Surface			
4.2	0.835	0.835	0.834	0.853
10.5	1.000	1.000	1.000	1.000
21.0	1.155	1.155	1.154	1.142
27.3	1.231	1.231	1.232	1.212
	1-cm depth			
4.2	0.859	0.859	0.859	0.859
10.5	1.000	1.000	1.000	1.000
21.0	1.065	1.065	1.065	1.065
27.3	1.081	1.081	1.081	1.081
	5-cm depth			
4.2	0.843	0.843	0.841	0.841
10.5	1.000	1.000	1.000	1.000
21.0	1.079	1.079	1.079	1.079
27.3	1.106	1.106	1.107	1.107
	Blue QED			
	Surface			
4.2	0.921	0.921	0.921	0.921
10.5	1.000	1.000	1.000	1.000
21.0	1.034	1.034	1.034	1.034
27.3	1.049	1.049	1.049	1.049
	1-cm depth			
4.2	0.903	0.903	0.903	0.903
10.5	1.000	1.000	1.000	1.000
21.0	1.021	1.021	1.021	1.021
27.3	1.065	1.065	1.065	1.065
	5-cm depth			
4.2	0.852	0.852	0.852	0.852
10.5	1.000	1.000	1.000	1.000
21.0	1.083	1.083	1.083	1.083
27.3	1.110	1.110	1.110	1.110

4. Discussion

Following the introduction of MR-IGRT to radiotherapy, understanding of the dosimeter response under the influence of magnetic fields has become important [33]. In this study, the effect of magnetic fields on QED detectors for clinical use was investigated as the presence of magnetic fields would significantly affect the black QED detectors for in vivo verification during treatment. The absolute response of the black QED detector changed according to the magnetic field direction, whereas that of the blue QED detector did not change. The blue QED detector was not affected by the magnetic field mainly because of its inherent build-up cover of 7.9-mm thickness. When photons interact with the patient's body, these contaminant electrons are generated

owing to Compton scattering. The contaminant electron generated on the surface of a patient can spread into the air. The energy of the contaminant electron is very low because it is the result of backward scattering. Despite this, it can form a stream owing to the direction of the magnetic field and will increase the surface dose. However, the contaminant electron cannot penetrate the build-up material (e.g., PMMA and aluminum) because of the low energy. Therefore, the blue QED with an inherent build-up region experiences no effect even with a magnetic field, while the effect is expected for the black QED without inherent build-up region.

The black QED detector showed a significant angular dependence, as reported in a previous study [25]. This dependence had a similar trend on the surface with and without magnetic fields. However, the trend shifted with the magnetic fields owing to the difference in the absolute value. The design of the QED detector and the back scattering from the phantom surface are the main factors that affect the angular dependence [34]. The QED detectors have a flat design for radiation incidence along the direction perpendicular to the plane of the die in accordance with the direction of the p-n junction. Therefore, a flat design has a larger angular dependency. To minimize the angular dependency, we have to ensure that the material and dimension of the buildup region are well designed. However, the black QED detector has no build-up cover, whereas the blue QED detector has an aluminum build-up cover with 0.41-cm thickness, as shown in Fig. 1. Therefore, the black QED detector has a significant angular dependence, whereas the blue QED detector has none. At gantry angles 90° and 270°, the response of both QED detectors decreased sharply. In setup 1, the incident beam could not make a full irradiation field at the phantom surface. Specifically, the angular dependence under setup 2 from Fig. 2 was greater at 90° and 270° owing to the arrangement of the detector and the connector. For the angular dependence of the blue QED detector, under setup 2, the response gradually decreased from gantry angles 280° to 80° because the cable area of the blue QED detector was affected by the radiation differently compared to that under setup 1. However, at 90° and 270° under setup 2, the radiation was irradiated directly through the cable of the detector and half of the radiation field was attenuated by a phantom. Therefore, the response of the detector dramatically decreased.

The angular dependence under setups 3 and 4 was also significant. For all angles, angular correction should be applied for clinical use. When radiation was applied to their back side (i.e., above 90°), the response of the QED detectors largely varied owing to the direction of the p-n junction and to the heterogeneous structures around the die. The response of the blue QED detector decreased sharply above 90° because the backscatter material changed. However, the dependence caused by magnetic field direction did not appear for every evaluated condition. In fact, the black QED detector located at 1 cm and 5 cm was not affected by the low-intensity magnetic field of 0.35 T.

In the case of setup 5 (i.e., angular variation between the detector and the magnetic field direction), the black QED detector showed a significant angular dependence. When the detector was placed at 90°, its response was minimal. The response increased from 90° to 180°. At 180°, the response was the same as that at 0°. As the black QED detector has no inherent build-up thickness, when it is attached to a phantom surface, even a low-intensity magnetic field affects its response. Such dependence was maximum at 90°, which is consistent with the Lorentz force, where the magnetic force is always perpendicular to the particle velocity [35]. In fact, the detector was perpendicular to the magnetic field of the ViewRay system, and, therefore, the maximum force was applied to the detector placed at 90°. In addition, the scatter electrons from the stem of the black QED detector directly affected the detector response, whereas the inherent build-up region of the blue QED detector absorbed such scatter electrons. In clinical practice, it would be difficult to apply specific corrections to different angles. Thus, aligning the detector on a patient's surface according to the calibration setup would render the correction for magnetic field direction unnecessary. The blue QED detector showed no dependence on the magnetic field direction given its build-up structure, and the magnetic field size and depth effects were negligible except for the measurements at the direction perpendicular to the magnetic field, where a slight impact was observed.

Sometimes, in vivo dosimetry is performed with a bolus as necessary. The variation on the depth was evaluated to determine the effect of the magnetic field for such a case. If the black QED detector was used with a 1-cm-thick bolus, the magnetic field showed no effect on it owing to the build-up. Even if the blue QED detector was used without a bolus (i.e., on the surface), the detector was not affected by the magnetic field. The response of the black QED detector upon varying the field size (i.e., output factor) at the surface was affected by the magnetic field. When the detector was used under the *parallel setup*, the absolute response decreased at the same rate as those for the four field sizes. In this case, the output factors were similar to those without a magnetic field, because all measurement values were normalized to the value of the reference field (i.e., field size of $10.5 \times 10.5\,cm^2$) for each measurement setup (i.e., the direction and present of magnetic field). In the case of the *perpendicular setup*, the output factor was slightly changed owing to the Lorentz force. Although the effect of the low-intensity magnetic field was negligible for the blue QED detector, the effect of the magnetic field was significant for the black QED detector attached to a phantom surface. Especially, the effect was greater under the perpendicular setup.

Such low-intensity magnetic fields may be applied in the ViewRay system during MRI as this presents some benefits [36,37]. For instance, it is easier to shield the magnet for the device performing the radiation delivery [38]. In addition, image acquisition is faster and presents fewer motion artifacts [38], and spatial distortion and signal loss from the metal can be significantly reduced. Moreover, the amount of energy deposited in tissues by radiofrequency pulses (i.e., specific absorption rate) is small [36,37]. However, several studies have shown that magnetic fields can affect some dosimeters (e.g., ion chambers, diode detectors, and optically stimulated luminescent dosimeters) under high-intensity magnetic fields in the order of 1.5 or 3 T [21,23,28]. Furthermore, LINAC systems using high-intensity magnetic fields are being developed and prepared for clinical use. Therefore, in future studies, the response of a QED detector for in vivo dosimetry under high-intensity magnetic fields will be evaluated.

5. Conclusion

We evaluated the effect of 0.35 T of magnetic field on QED detectors. The impact of such low-intensity field was limited for the blue QED detector, and, thus, no correction is required in most clinical situations for this detector. However, when the black QED detector was placed on a patient' surface, its response was decreased by the magnetic field. Moreover, correction should be performed for the angle between the detector alignment and the magnetic field direction. The effect of the magnetic field increased and field size dependency was shown for the *perpendicular setup*. Therefore, if calibration is performed without any magnetic field, the response in the magnetic field should be corrected. We recommend that the black QED detector be placed parallel to the magnetic field on a patient's surface (i.e., same position as that in the calibration setup) to avoid the need for additional correction in clinical use.

Conflicts of interest statement

The authors declare that they have no competing interests.

Acknowledgments

Funding: This work was supported by the National R&D Program for Cancer Control by the Ministry of Health and Welfare, Republic of

Korea (HA16C0025).

References

[1] Park J, Kim K, Chie E, Choi C, Ye S, Ha S. RapidArc® vs intensity-modulated radiation therapy for hepatocellular carcinoma: a comparative planning study. Br J Radiol 2012;85:e323–9.

[2] Quan EM, Li X, Li Y, Wang X, Kudchadker RJ, Johnson JL, et al. A comprehensive comparison of IMRT and VMAT plan quality for prostate cancer treatment. Int J Radiat Oncol Biol Phys 2012;83:1169–78.

[3] Smit C, Shaw W. An investigation of dose and quality in clinical IGRT imaging protocols. Phys Med: Eur J Med Phys 2015;31:S12.

[4] Hu Y, Rankine L, Green OL, Kashani R, Li HH, Li H, et al. Characterization of the onboard imaging unit for the first clinical magnetic resonance image guided radiation therapy system. Med Phys 2015;42:5828–37.

[5] Delishaj D, Ursino S, Pasqualetti F, Matteucci F, Cristaudo A, Soatti CP, et al. Set-up errors in head and neck cancer treated with IMRT technique assessed by cone-beam computed tomography: a feasible protocol. Radiat Oncol J 2018;36:54.

[6] Lee SY, Lim S, Ma SY, Yu J. Gross tumor volume dependency on phase sorting methods of four-dimensional computed tomography images for lung cancer. Radiat Oncol J 2017;35:274.

[7] Yahalom J, Illidge T, Specht L, Hoppe RT, Li Y-X, Tsang R, et al. Modern radiation therapy for extranodal lymphomas: field and dose guidelines from the international lymphoma radiation oncology group. Int J Radiat Oncol Biol Phys 2015;92:11–31.

[8] Mutic S, Low D, Chmielewski T, Fought G, Gerganov G, Hernandez M, et al. The design and implementation of a novel compact linear accelerator-based magnetic resonance imaging-guided radiation therapy (MR-IGRT) system. Int J Radiat Oncol Biol Phys 2016;96:E641.

[9] Lee HJ, Kadbi M, Bosco G, Ibbott GS. Real-time volumetric relative dosimetry for magnetic resonance—image-guided radiation therapy (MR-IGRT). Phys Med Biol 2018;63:045021.

[10] Raaymakers B, Jürgenliemk-Schulz I, Bol G, Glitzner M, Kotte A, van Asselen B, et al. First patients treated with a 1.5 T MRI-Linac: clinical proof of concept of a high-precision, high-field MRI guided radiotherapy treatment. Phys Med Biol 2017;62:L41.

[11] Feygelman V, Lohr F, Orton CG. The future of MRI in radiation therapy belongs to integrated MRI-linac systems, not the standalone MRI-Sim. Med Phys 2017;44:791–4.

[12] Nguyen D, Thomas D, Cao M, O'Connor D, Lamb J, Sheng K. Computerized triplet beam orientation optimization for MRI-guided Co-60 radiotherapy. Med Phys. 2016;43:5667–75.

[13] Park JM, Park S-Y, Wu H-G, J-i Kim. Commissioning experience of tri-cobalt-60 MRI-guided radiation therapy system. Prog Med Phys 2015;26:193–200.

[14] Cho JD, Park JM, Choi CH, Wu H-G, Kim J-i, Park S-Y. Implementation of AAPM's TG-51 protocol on Co-60 MRI-guided radiation therapy system. Prog Med Phys 2017;28:190–6.

[15] Park JM, Park S-Y, Kim J-I, Kang H-C, Choi CH. A comparison of treatment plan quality between Tri-Co-60 intensity modulated radiation therapy and volumetric modulated arc therapy for cervical cancer. Phys Med 2017;40:11–6.

[16] Choi CH, Park S-Y, Kim J-I, Kim JH, Kim K, Carlson J, et al. Quality of tri-Co-60 MR-IGRT treatment plans in comparison with VMAT treatment plans for spine SABR. Br J Radiol 2016;90:20160652.

[17] Park JM, Park S-Y, Choi CH, Chun M, Kim JH, Kim J-I. Treatment plan comparison between Tri-Co-60 magnetic-resonance image-guided radiation therapy and volumetric modulated arc therapy for prostate cancer. Oncotarget 2017;8:91174.

[18] Merna C, Rwigema J-CM, Cao M, Wang P-C, Kishan AU, Michailian A, et al. A treatment planning comparison between modulated tri-cobalt-60 teletherapy and linear accelerator-based stereotactic body radiotherapy for central early-stage non-small cell lung cancer. Med Dosim 2016;41:87–91.

[19] Park JM, Park S-Y, Kim HJ, Wu H-G, Carlson J, Kim J-I. A comparative planning study for lung SABR between tri-Co-60 magnetic resonance image guided radiation therapy system and volumetric modulated arc therapy. Radiother Oncol 2016;120:279–85.

[20] Reynoso FJ, Curcuru A, Green O, Mutic S, Das IJ, Santanam L. Magnetic field effects on Gafchromic-film response in MR-IGRT. Med Phys 2016;43:6552–6.

[21] Spindeldreier C, Schrenk O, Ahmed M, Shrestha N, Karger C, Greilich S, et al. Feasibility of dosimetry with optically stimulated luminescence detectors in magnetic fields. Radiat Meas 2017;106:346–51.

[22] Lee HJ, Roed Y, Venkataraman S, Carroll M, Ibbott GS. Investigation of magnetic field effects on the dose–response of 3D dosimeters for magnetic resonance–image guided radiation therapy applications. Radiother Oncol 2017;125:426–32.

[23] O'Brien D, Roberts D, Ibbott G, Sawakuchi G. Reference dosimetry in magnetic fields: formalism and ionization chamber correction factors. Med Phys 2016;43:4915–27.

[24] Reynolds M, Fallone B, Rathee S. Response measurement for select radiation detectors in magnetic fields. Med Phys 2015;42:2837–40.

[25] Colussi VC, Beddar AS, Kinsella TJ, Sibata CH. In vivo dosimetry using a single diode for megavoltage photon beam radiotherapy: Implementation and response characterization. J Appl Clin Med Phys 2001;2:210–8.

[26] Essers M, Mijnheer. In vivo dosimetry during external photon beam radiotherapy. Int J Radiat Oncol Biol Phys 1999;43:245–59.

[27] Lee J, Kim I, Park J-W, Lim Y-K, Moon M, Lee S, et al. Development of diode based high energy X-ray spatial dose distribution measuring device. J Radiat Protect 2018;43:97–106.

[28] O'Brien DJ, Dolan J, Pencea S, Schupp N, Sawakuchi GO. Relative dosimetry with an MR-linac: response of ion chambers, diamond, and diode detectors for off-axis, depth dose, and output factor measurements. Med Phys 2018;45:884–97.

[29] Saini AS, Zhu TC. Temperature dependence of commercially available diode detectors. Med Phys 2002;29:622–30.

[30] Zhu X. Entrance dose measurements for in-vivo diode dosimetry: Comparison of correction factors for two types of commercial silicon diode detectors. J Appl Clin Med Phys 2000;1:100–7.

[31] Hackett SL, Van Asselen B, Wolthaus JW, Bluemink JJ, Ishakoglu K, Kok J, et al. Spiraling contaminant electrons increase doses to surfaces outside the photon beam of an MRI-linac with a perpendicular magnetic field. Phys Med Biol 2018;63(9):095001.

[32] Sun Nuclear Corporation. QED™ Detector User's Guide.

[33] Raaijmakers A, Raaymakers BW, Lagendijk JJ. Magnetic-field-induced dose effects in MR-guided radiotherapy systems: dependence on the magnetic field strength. Phys Med Biol 2008;53:909.

[34] Saini AS. In-vivo radiation diode dosimetry for therapeutic photon beams [Graduate Theses and Dissertations]. University of South Florida; 2007.

[35] Van Zijp H, Van Asselen B, Wolthaus J, Kok J, De Vries J, Ishakoglu K, et al. Minimizing the magnetic field effect in MR-linac specific QA-tests: the use of electron dense materials. Phys Med Biol 2016;61:N50.

[36] Mutic S, Dempsey JF. The ViewRay system: magnetic resonance–guided and controlled radiotherapy. Sem Radiat Oncol 2014;24:196–9.

[37] Noel CE, Parikh PJ, Spencer CR, Green OL, Hu Y, Mutic S, et al. Comparison of onboard low-field magnetic resonance imaging versus onboard computed tomography for anatomy visualization in radiotherapy. Acta Oncol 2015;54:1474–82.

[38] Jaffray D, Carlone M, Menard C, Breen S. Image-guided radiation therapy: Emergence of MR-guided radiation treatment (MRgRT) systems. Phys Med Imag: Int Soc Opt Photon 2010;7622:762202.